

# Nonequilibrium Dynamics of Gating-Induced Resistance Transition in Charge Density Wave Insulators

Sheng Zhang<sup>1</sup> and Gia-Wei Chern<sup>1</sup>

<sup>1</sup>*Department of Physics, University of Virginia, Charlottesville, VA 22904, USA*

(Dated: January 7, 2022)

We present a comprehensive numerical study of the gating-induced insulator-to-metal transition in the charge density wave (CDW) state of the Holstein model. Large-scale Brownian dynamics method with forces computed from nonequilibrium Green's function method is employed to simulate the spatio-temporal dynamics of the CDW state. We show that a threshold voltage, determined by the energy of the in-gap edge modes, is required to induce the instability of the CDW. A large bias voltage, on the other hand, induces a sudden transition to the metallic state similar to a dielectric breakdown. At intermediate voltages, our extensive simulations show that the transition to the low-resistance state is initiated by the nucleation of a thin conducting layer at the gating electrode. The resultant metal-insulator interface is then swept over the system by the voltage bias, resulting in a growing metallic domain. We further characterize the voltage and temperature dependence of the domain-wall dynamics.

Complex adaptive materials with multiple resistant states are widely exploited as building blocks for next generation electronic and information technology. The operation of conventional metal-oxide semiconductor field-effect transistors (MOSFET) relies on the electrostatic charging of free electrons in thermal equilibrium, leading to a switching speed bounded by 60 mV per decade, also known as the Boltzmann limit. In contrast, controllable switching between many-body states with different resistances offers the possibility of high-speed and low-power transistor operations. In particular, it has been suggested that ultrafast switching can be achieved by the collective response of electrons in an insulator-to-metal transition (IMT) [1–3]. Indeed, an emerging technology called the “Motronics” aims at achieving electronic and logical operations by controlling electron correlation in the Mott insulators [4–6]. The high-resistant state of these materials results from the localization of electrons due to the short-range Coulomb repulsion. The Mott insulator can be induced to a low-resistant state via a first-order transition by reducing the electron repulsive energy through electrostatic doping.

A charge density wave (CDW) state [7–9] is another many-body state that attracts enormous attention due to their potential electronic and optoelectronic applications. A CDW phase is a macroscopic quantum state consisting of a periodic modulation of the electronic charge density accompanied by a periodic structural distortion. Early interests in CDW focused on the sliding phase of the quasi-one-dimensional incommensurate states with nonlinear conductivity at low applied voltage [8]. Other novel properties include giant dielectric response, multi-stable conducting states, and proximity to unusual superconductivity. The interest in CDW is rekindled in recently years due to the advent of quasi-2D van der Waals materials, where CDW phases can manifest themselves at room temperatures and above [10–18]. Moreover, as these CDW phases can be readily manipulated

by temperature, strain, bias voltage, and other stimuli, these quasi-2D CDW materials are emerging as a new paradigm for multifunctional devices.

In particular, electrically induced transitions between different CDW phases, as well as CDW-metal transitions have been demonstrated in the 1T polymorph of tantalum disulfide (TaS<sub>2</sub>) [19–24], with a timescale of a few nanoseconds, making this material a promising candidate for high-speed energy-efficient electronic applications [24–26]. The voltage or electric field induced IMT or resistive transition is known to be a highly complex process which involves a large variety of microscopic mechanisms including carrier dynamics, lattice distortions, heat transport, and electron correlation effect. The electrical switching from CDW to metallic state is no exception. On the other hand, recent experiments indicated that this process is driven mainly by motion of complex domain walls [20] and is qualitatively different from the resistive switching in complex oxides or chalcogenide glass which are characterized by highly inhomogeneous intermediate states [27–33].

Despite its fundamental importance and technological implications, theoretical modeling of the electrically induced CDW transitions remains mostly at the phenomenological level. This is understandably a difficult task due to the multi-scale nature of the problem. On one hand, one needs to describe the dynamical evolution of the lattice degrees of freedom, while accounting for the nonequilibrium nature of the electron system. On the other hand, large-scale real-space simulation is required in order to capture the transient pattern formation and domain-wall propagation. Finally, for systems with strong electron correlation, the need of proper many-body techniques further adds the computational complexity.

In this paper, we present the first-ever large-scale dynamical simulations of the CDW phase transition, focusing on the interplay of lattice dynamics and the influence

of the out-of-equilibrium electrons. We consider the adiabatic limit of the Holstein model in which the lattice degrees of freedom can be treated as classical variables, and the model can then be exactly solved numerically. By performing large-scale quantum Brownian dynamics simulation with the forces computed from the nonequilibrium Green's function method, we demonstrate a reversible gating-induced CDW-to-metal transition that is driven by the domain-wall motion. We further obtain a dynamical phase diagram and characterize the voltage and temperature dependence of the domain-wall dynamics.

We consider a capacitor structure with a square-lattice Holstein model sandwiched by two electrodes shown in Fig. 1(a). The right electrode serves as the substrate, while a gate voltage  $V$  is applied at the left electrode. The total Hamiltonian of the system is  $\mathcal{H} = \mathcal{H}_{\text{Hols}} + \mathcal{H}_{\text{res}}$ , where  $\mathcal{H}_{\text{Hols}}$  is the Holstein Hamiltonian for the square-lattice in the center, and  $\mathcal{H}_{\text{res}}$  describes the electrodes, reservoir degrees of freedom. The Holstein Hamiltonian reads [34]

$$\hat{\mathcal{H}}_{\text{Hols}} = -t_{\text{nn}} \sum_{\langle ij \rangle} \hat{c}_i^\dagger \hat{c}_j - g \sum_i Q_i \left( \hat{n}_i - \frac{1}{2} \right) \quad (1)$$

where  $\hat{c}_i/\hat{c}_i^\dagger$  is the annihilation/creation operators of spinless electron at site- $i$ , and  $\hat{n}_i \equiv \hat{c}_i^\dagger \hat{c}_i$  is the corresponding number operator,  $Q_i$  describes a local structural distortion at site- $i$ , such as the breathing mode of the oxygen octahedron. The first-term describes nearest-neighbor hopping  $t_{\text{nn}}$  of electrons, and the second term denotes phonon-electron interaction with a coupling constant  $g$ . As discussed above, here we treat the Holstein phonon  $Q_i$  as classical variables with the following elastic energy [34]

$$\mathcal{V} = \frac{k}{2} \sum_i Q_i^2 + \sum_{\langle ij \rangle} \kappa Q_i Q_j, \quad (2)$$

where  $k$  is the effective on-site spring constant, and  $\kappa$  describes a nearest-neighbor repulsion between the local distortions. The Holstein model is one of the most studied electron-phonon model systems, and is widely used to investigate the physics of polarons, superconductivity, and CDWs [35–43]. In the adiabatic limit, similar to the Born-Oppenheimer approximation widely used in quantum or *ab initio* molecular dynamics [46], the electron relaxation is assumed to be much faster than the lattice dynamics. To this end, we employ an over-damped Langevin dynamics, or the Brownian dynamics (BD) to model the time evolution of the lattice distortions [43–45]

$$\frac{dQ_i}{dt} = -\frac{1}{\gamma} F_i + \zeta_i(t), \quad (3)$$

where  $\gamma$  is an effective friction constant, and  $\zeta_i(t)$  denotes a stochastic force described by a delta-correlated

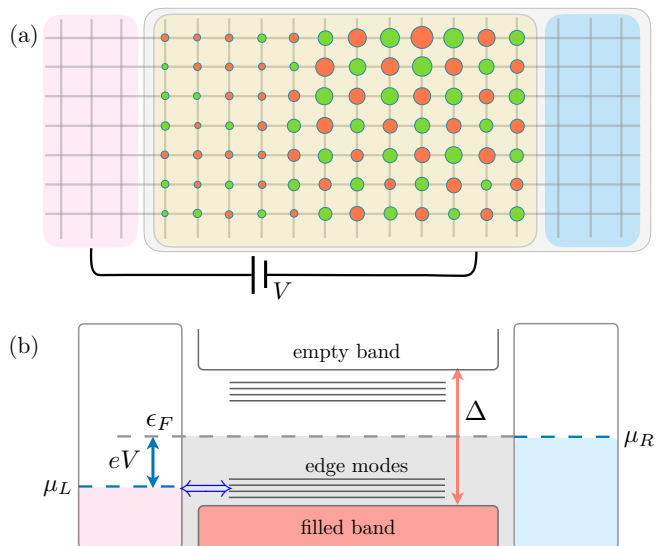


FIG. 1: (Color online) (a) Schematic diagram of the Gating-induced CDW to metal transition in the adiabatic Holstein model. (b) Energy diagram of the two electrodes and the center Holstein model. The CDW state is a band insulator with an energy gap  $E_g = 2gQ_0$ . Both the Fermi level  $\epsilon_F$  at the bulk and the chemical potential  $\mu_R$  of the right electrode are set at the middle of the energy gap, while the chemical potential of the left-electrode is lowered from the Fermi level by the gating voltage:  $\mu_L = \epsilon_F - eV$ .

stationary Gaussian process. The driving force of a conservative system is given by the derivative of a potential energy:  $F = -\partial E/\partial Q_i$ . For electron forces in thermal equilibrium, the effective energy is given by  $E = \langle \hat{\mathcal{H}}_{\text{Hols}} \rangle = \text{Tr}(\hat{\rho}_{\text{eq}} \hat{\mathcal{H}}_{\text{Hols}})$ . However, for a driven electronic system, the energy is not well defined, and the force in general is non-conservative. Nonetheless, the force can still be obtained from a generalized Hellmann-Feynman theorem [47–51]

$$F_i = -\left\langle \frac{\partial \hat{\mathcal{H}}_{\text{Hols}}}{\partial Q_i} \right\rangle = g \langle \hat{n}_i \rangle \quad (4)$$

where the expectation value  $\langle \dots \rangle$  is evaluated with respect to the quasi-steady-state, yet out-of-equilibrium, electron subsystem.

We next employ the nonequilibrium Green's function (NEGF) method [52–55] to compute these expectation values. To this end, we consider the following explicit Hamiltonian for the electrodes and reservoir

$$\mathcal{H}_{\text{res}} = \sum_{\xi, i} \epsilon_\xi d_{i, \xi}^\dagger d_{i, \xi} - \sum_{i, \xi} V_{\xi, i} (d_{i, \xi}^\dagger c_i + \text{h.c.}). \quad (5)$$

Here  $d_{i, \xi}$  represents non-interacting fermions from the bath ( $i$  inside the bulk) or the leads (for  $i$  on the two open boundaries), and  $\xi$  is a continuous quantum number. For example,  $\xi$  can be used to represent the band-structure of the two leads. After integrating out the reservoir fermions in both leads and bath, the retarded

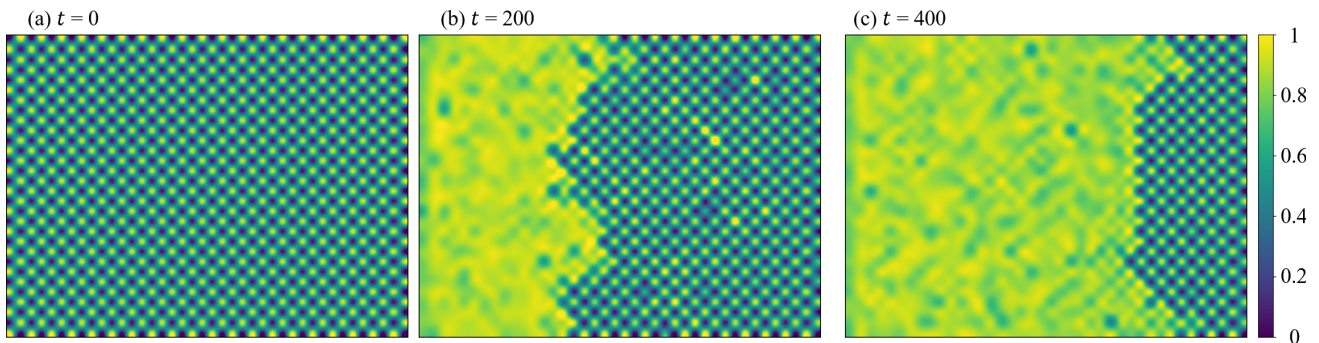


FIG. 2: (Color online) NEGF-BD simulations of a driven Holstein model on a  $40 \times 30$  square lattice. The driven voltage is applied along the longitudinal  $x$  direction. Panels (a)–(c) show the snapshots of the system local electron density  $n_i = \langle \hat{c}_i^\dagger \hat{c}_i \rangle$  at various simulation times. The following parameters are used: electron-phonon coupling constant  $g = 1.5t_{\text{nn}}$ , the effective spring constant  $k_1 = 0.67g$ , nearest-neighbor elastic coupling  $\kappa = 0.12g$ , damping constant  $\lambda = 0.2g$ ,  $\Gamma_{\text{lead}} = 1.0$ ,  $\Gamma_{\text{bath}} = 0.001$ ,  $k_B T = 0.1$ , and the bias voltage  $eV = 2.5t_{\text{nn}}$ .

Green's function matrix for the central region is given by  $\mathbf{G}^r(\epsilon) = (\epsilon \mathbf{I} - \mathbf{H} - \mathbf{\Sigma}^r)^{-1}$ , where  $H_{ij} = t_{ij} - g\delta_{ij}Q_i$  is the tight-binding matrix of the Holstein model Eq. (1) and

$$\Sigma_{ij}^r(\epsilon) = \delta_{ij} \sum_{\xi} |V_{i,\xi}|^2 / (\epsilon - \epsilon_{\xi} + i0^+) \quad (6)$$

is the dissipation-induced self-energy. The resultant level-broadening matrix given by  $\mathbf{\Gamma} = i(\mathbf{\Sigma}^r - \mathbf{\Sigma}^a)$  is diagonal with  $\Gamma_{ii} = \pi \sum_{\xi} |V_{i,\xi}|^2 \delta(\epsilon - \epsilon_{\xi})$ . For simplicity, we assume flat wide-band spectrum for the reservoirs, which leads to a frequency-independent broadening factor. Next, using the Keldysh formula, the lesser Green's function is obtained from the retarded/advanced Green's functions:  $\mathbf{G}^<(\epsilon) = \mathbf{G}^r(\epsilon) \mathbf{\Sigma}^<(\epsilon) \mathbf{G}^a(\epsilon)$ , and the lesser self-energy is related to the  $\Sigma^{r/a}$  through dissipation-fluctuation theorem:  $\Sigma_{ij}^<(\epsilon) = 2i \delta_{ij} \Gamma_i f_{\text{FD}}(\epsilon - \mu_i)$ . Here  $\Gamma_i = \Gamma_{\text{lead}}$  or  $\Gamma_{\text{bath}}$  depending on whether site- $i$  is at the boundaries or in the bulk. The local chemical potential  $\mu_i = \epsilon_F$  for the bath, and  $\mu_i = \mu_{L/R}$  for the two electrodes. Finally, the nonequilibrium force in Eq. (4) is proportional to the on-site electron density  $\langle \hat{n}_i \rangle = \langle \hat{c}_i^\dagger(t) \hat{c}_i(t) \rangle$ , which is the diagonal element of the equal-time lesser Green's function

$$F_i(t) = g G_{ii}^<(t, t) = g \int_{-\infty}^{+\infty} G_{ii}^<(\epsilon; t) d\epsilon. \quad (7)$$

In our implementation, the integral is replaced by a Riemann summation with an  $\Delta\epsilon = 0.003$ , i.e. with up to 4000 energy values in the summation.

We apply the NEGF-BD method outline above to simulate the gating-induced IMT of the Holstein model on a  $40 \times 30$  lattice. The initial state of the simulations was obtained first using the equilibrium Brownian dynamics simulations with half-filled electrons  $\bar{n} \equiv \sum_i \hat{n}_i / N = 0.5$  per site. This results in an initial state with CDW order on the square lattice; see Fig. 2(a). The band structure a perfect CDW order is given by  $E_{\pm}(\mathbf{k}) = \pm \sqrt{\epsilon_{\mathbf{k}}^2 + g^2 Q_0^2}$ , where  $\epsilon_{\mathbf{k}}$  is the energy dispersion of the square-lattice

tight-binding Hamiltonian, and  $Q_0$  is the amplitude of the lattice distortion in the CDW state. Importantly, an energy gap  $\Delta = 2gQ_0$  is opened in the spectrum. At half-filling, the valance band  $E_-(\mathbf{k})$  is completely filled, and the Holstein model is in a band-insulator state.

Next we turn on the voltage bias  $V$ . As illustrated in Fig. 1(b), the chemical potential of both the substrate (the right electrode) and the center square lattice is kept at the zero  $\epsilon_F = \mu_R = 0$ , which is set at the middle of the energy gap, while that of the left electrode is  $\mu_L = -eV$ . Fig. 2 shows an example of the phase transformation of the Holstein system driven by a gating voltage  $eV = 2.5$ . The color gradient shows the expectation value of the on-site density  $\langle \hat{n}_i \rangle$ . Other simulation parameters are: electron-phonon coupling constant  $g = 1.5t_{\text{nn}}$ , local displacement  $Q_i$  string constant  $k_1 = 0.67g$ , nearest-neighbor coefficient  $\kappa = 0.12g$ , damping constant  $\lambda = 0.2g$ ,  $\Gamma_{\text{lead}} = 1.0$ ,  $\Gamma_{\text{bath}} = 0.001$ , and the temperature is  $k_B T = 0.1$ .

As shown in Fig. 2, the gating voltage induces an instability of the CDW, which results in the formation of a metallic domain as the electrons are drained from the gating electrode with a lower chemical potential. The resultant CDW-metallic domain wall is then driven to the substrate. To further characterize the phase transformation process, we compute the transmission current of the driven electron state [52–55]

$$I = \int \text{Tr}(\mathbf{\Gamma}_R \mathbf{G}^r \mathbf{\Gamma}_L \mathbf{G}^a) [f_L(\epsilon) - f_R(\epsilon)] d\epsilon, \quad (8)$$

where  $\mathbf{\Gamma}_{L,R}$  are the diagonal broadening matrices, and  $f_{L,R}(\epsilon) = f_{\text{FD}}(\epsilon - \mu_{L,R})$  are the Fermi-Dirac functions. Fig. 3(a) shows the transmission current  $I$  as a function of time under a bias voltage  $eV = 2.5$  at a temperature  $T \rightarrow 0$ . The roughly linear segment in the semi-log plot indicates an exponential growth of the current:  $I \sim \exp(ct)$ , where  $c$  is a numerical constant. We note that the phase transformation at such low temperatures is essentially a downhill process, with energy dissipated

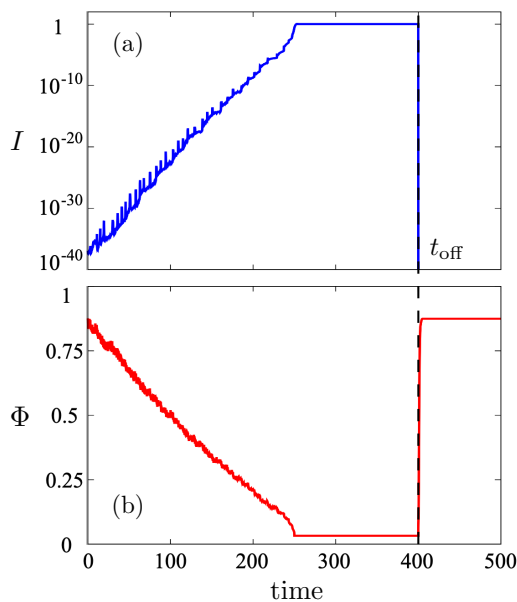


FIG. 3: (Color online) Time dependence of (a) the transmission current  $I$  and (b) the CDW order parameter  $\Phi$  at zero temperature. A constant voltage  $eV = 2.5t_{\text{nn}}$  is applied to the Holstein system during the interval  $0 \leq t \leq t_{\text{off}} = 400$ .

away both through the effective damping  $\gamma$  of the lattice, and the electron reservoir. Interestingly, as the CDW-metal interface moves across the sample one layer at a time, this discrete procession gives rise to the small spikes on top of the exponential increase in the figure. Fig. 3(b) shows the time dependence of the CDW order parameter, which is defined as

$$\Phi = \sum_i \langle \hat{n}_i \rangle \exp(i\mathbf{Q} \cdot \mathbf{r}_i), \quad (9)$$

where  $\mathbf{Q}_i = (\pi/a, \pi/a)$  is the wave vector characterizing the checkerboard pattern on the square lattice. The almost linear decrease of  $\Phi$  during the phase transformation indicates an almost linear propagation of the CDW-metal domain wall.

Our simulations also show that the metallic state is stable only in the presence of the bias voltage, which means that the insulator-metal transition is reversible. This is demonstrated in Fig. 3 which shows that the CDW order returns to its initial value when the gating voltage is turned off. Interestingly, contrary to the voltage-driven transition which proceeds through intermediate states with propagating domain-wall, the recovery to the CDW state is almost immediate, indicating a bulk instability. It is worth noting that the fact that the CDW order resumes to its initial maximum value in our simulation is a finite-size effect. For large lattices, the reverse transition is likely to result in the formation of multiple CDW domains of opposite signs.

We next investigate the effects of the gate voltage on the phase transformation rate. Fig. 4(a) shows the aver-

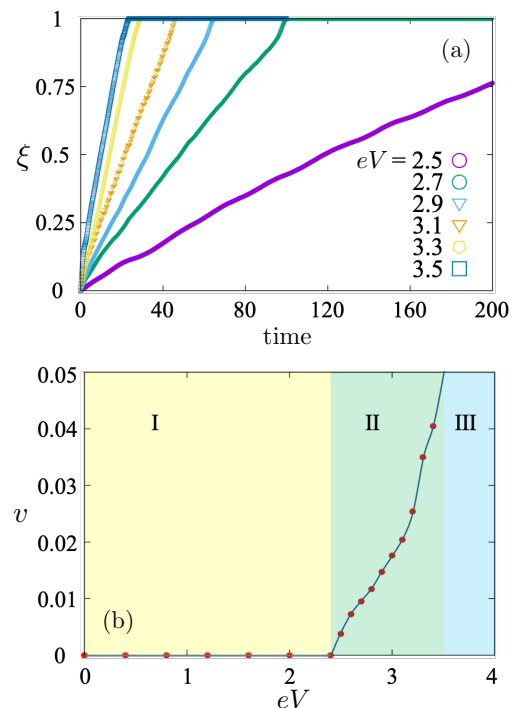


FIG. 4: (Color online) (a) average position  $\xi$  of the CDW-metal domain-wall as a function of time for different gating voltages at zero temperature. (b) CDW-metal domain-wall velocity  $v$  as a function of the gate voltage  $eV$ . The velocity is computed from the average slope of the  $\xi(t)$  curve in panel (a).

age position  $\xi$  of the CDW-metal interface as a function of time at different bias voltage. As expected, a larger gate voltage results in faster domain-wall motion. The average velocity of the interface, obtained through a linear fitting of the domain-wall trajectory  $\xi(t)$ , is plotted in Fig. 4(b) as a function of the bias voltage. Importantly, one can identify three different dynamical regimes from this result. For gate voltage smaller than a threshold  $eV_{\text{th}} \sim 2.4$ , the CDW remains a stable state. In regime-II, a voltage-induced instability results in the formation of CDW-metal interface whose propagation velocity increases with larger voltage. And finally, for  $V$  greater than a second critical value, the transition to the metallic phase takes place instantly through a process similar to a dielectric breakdown.

This dynamical phase diagram can be understood from the energy diagram shown in Fig. 1(b), which also provides an explanation of the phase transition mechanisms. For a small bias voltage the chemical potential of the gating electrode  $\mu_L$  lies in the energy gap of the CDW state and, as a result, is ineffective in inducing the phase transition. As the voltage is increased to a point that  $\mu_L$  overlaps with the energy levels of the in-gap states that are localized at the left edge, the resonant coupling leads to an instability of the CDW. As electrons are drained from the gate due to a smaller chemical potential, a metallic layer is nucleated near the left edge. The phase transforma-



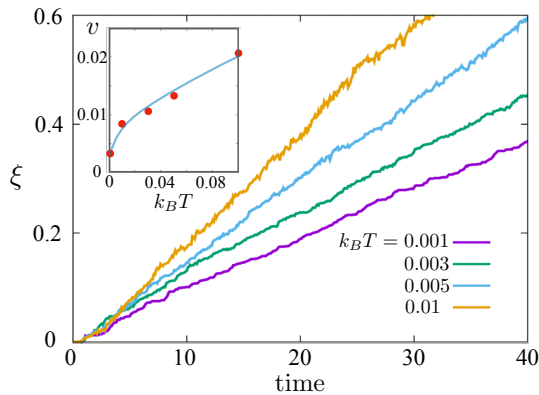


FIG. 5: (Color online) Average position  $\xi$  of the CDW-metal interface as a function of time for different temperatures with constant driven voltage  $eV = 2.5t_{nn}$ . The inset shows the CDW-metal domain-wall velocity as a function of temperature.

tion then proceeds through the expansion of the metallic domain. This corresponds to the dynamical regime-II in Fig. 4(b). As the applied voltage is further increased such that the chemical potential  $\mu_L$  is lower than the valance band-edge, the gate electrode now directly couples to the energy states in the bulk, thus allowing efficient current flow through the bulk and an instant instability toward the metallic phase.

The domain-wall propagation at  $T \rightarrow 0$  discussed above is governed by a relaxation dynamics dominated by the dissipation of energy. It is worth noting that the effective potential of the local lattice distortion is similar to a double-well potential, with one minimum at  $Q_i = \pm Q_0$  (depending on the sublattice) and the other one at  $Q_i \sim 0$  corresponding to the metallic phase. The energy surface of the whole system is more complicated than this simple picture. The layer-by-layer progression the metallic domain indicates that each domain-wall position is a quasi-stable state in the high dimensional configuration space. As more energy is drained from the gate, the decay of a local minimum leads to the advance of the domain-wall by one layer. In the presence of thermal fluctuations, the system can jump from one local minimum to the next one through thermal tunneling, instead of waiting for the decay of the present minimum. It is thus expected that the domain-wall mobility is enhanced at finite temperatures. This is indeed confirmed in our simulations, as shown in Fig. 5. Except for the point at very low temperature, we find an approximate linear increase of the domain-wall velocity with temperature.

In conclusion, we have carried out large-scale NEGF-Brownian dynamics simulations to investigate the gating-induced CDW to metal transition in a well-studied electron-phonon system. In addition to the well-known electrical breakdown scenario at large bias voltages, we uncover a transformation process characterized by metastable states with propagating metal-insulator domain-

walls at intermediate voltages. The initial instability of the CDW in this intermediate dynamical regime is caused by the nucleation of a metallic layer at the gating electrode. The resultant metal-CDW interface propagates through the system with an approximately constant velocity that increases with the voltage bias and the temperature. Moreover, the voltage-induced transition is reversible; the system undergoes an instant transformation back to the CDW state when the gating voltage is removed.

Our work focuses on the interplay between atomic lattice dynamics and the out-of-equilibrium electrons. Importantly, our study uncovers the instability mechanisms for the CDW states. Nonetheless, the CDW phase transition in real materials, such as the quasi-2D van der Waals materials, is a highly complex process which is beyond the present work. In particular, by focusing on the solvable Holstein model in the adiabatic limit, our simulations neglect the electron correlation effect, which is likely to be important in compounds such as 1T-TaS<sub>2</sub> that is intensively studied experimentally. Many-body techniques such as Hartree-Fock or Gutzwiller are required to properly model the collective electron behaviors in CDW described by, e.g. the Holstein-Hubbard model [56, 57]. For example, self-consistent Hartree-Fock equation combined with NEGF was used to investigate the complex spin-density wave patterns in voltage-driven Hubbard model [58–60]. However, a full dynamical modeling of CDW transitions requires further integration with real-space lattice dynamics, which is computationally highly demanding. Machine-learning methods could provide a promising solution for the multi-scale modeling of the complex CDW dynamics.

The author thanks G. Kotliar, and Jong Han for fruitful discussions. This work is supported by the US Department of Energy Basic Energy Sciences under Award No. DE-SC0020330. The author also acknowledge the support of Advanced Research Computing Services at the University of Virginia.

- 
- [1] N. F. Mott, *Metal-Insulator Transitions* (Taylor & Francis, New York, 1997).
  - [2] M. Imada, A. Fujimori, and Y. Tokura, Metal-insulator transitions, *Rev. Mod. Phys.* **70**, 1039 (1998).
  - [3] V. Dobrosavljevic, *Introduction to Metal-Insulator Transitions* (Oxford University Press, Oxford, 2012).
  - [4] M. Nakano, K. Shibuya, D. Okuyama, T. Hatano, S. Ono, M. Kawasaki, Y. Iwasa, and Y. Tokura, Collective bulk carrier delocalization driven by electrostatic surface charge accumulation, *Nature* **487**, 459 (2012).
  - [5] N. Shukla, A. V. Thathachary, A. Agrawal, H. Paik, A. Aziz, D. G. Schlom, S. K. Gupta, R. Engel-Herbert, and S. Datta, A steep-slope transistor based on abrupt electronic phase transition, *Nat. Commun.* **6**, 7812 (2015).

- [6] J. Song, J. Woo, S. Lee, and A. Prakash, *IEEE Electron Device Lett.* **37**, 932 (2016).
- [7] G. Grüner, The dynamics of charge-density waves, *Rev. Mod. Phys.* **60**, 1129 (1988).
- [8] R. E. Thorne, Charge-Density-Wave Conductors, *Phys. Today* **49**, 42 (1996).
- [9] A. A. Balandin, S. V. Zaitsev-Zotov, and G. Grüner, Charge-density-wave quantum materials and devices – New developments and future prospects, *Appl. Phys. Lett.* **119**, 170401 (2021).
- [10] M. Porer, U. Leierseder, J.-M. Ménard, H. Dachraoui, L. Mouchliadis, I. E. Perakis, U. Heinzmann, J. Demsar, K. Rossnagel, and R. Huber, Non-thermal separation of electronic and structural orders in a persisting charge density wave, *Nat. Mater.* **13**, 857 (2014).
- [11] L. Stojchevska, I. Vaskivskiy, T. Mertelj, P. Kusar, D. Svetin, S. Brazovskii, D. Mihailovic, Ultrafast Switching to a Stable Hidden Quantum State in an Electronic Crystal, *Science* **344**, 177 (2014).
- [12] Y. Yu, F. Yang, X.F. Lu, Y.J. Yan, Y.-H. Cho, L. Ma, X. Niu, S. Kim, Y.-W. Son, D. Feng, S. Li, S.-W. Cheong, X.H. Chen, and Y. Zhang, Gate-tunable phase transitions in thin flakes of 1T-TaS<sub>2</sub>, *Nat. Nanotech.* **10**, 270 (2015).
- [13] I. Vaskivskiy, J. Gospodaric, S. Brazovskii, D. Svetin, P. Sutar, E. Goreshnik, I. A. Mihailovic, T. Mertelj, D. Mihailovic, Controlling the metal-to-insulator relaxation of the metastable hidden quantum state in 1T-TaS<sub>2</sub>, *Sci. Adv.* **1**, e1500168 (2015).
- [14] R. Samnakay, D. Wickramaratne, T. R. Pope, R. K. Lake, T. T. Salguero, and A. A. Balandin, *Nano Lett.* **15**, 2965 (2015).
- [15] X. Xi, L. Zhao, Z. Wang, H. Berger, L. Forró, J. Shan, and K. F. Mak, Strongly enhanced charge-density-wave order in monolayer NbSe<sub>2</sub>, *Nat. Nanotechnol.* **10**, 765 (2015).
- [16] D. Cho, S. Cheon, K.-S. Kim, S.-H. Lee, Y.-H. Cho, S.-W. Cheong, and H. W. Yeom, Nanoscale manipulation of the Mott insulating state coupled to charge order in 1T-TaS<sub>2</sub>, *Nat. Commun.* **7**, 10453 (2016).
- [17] S. Vogelgesang, G. Storeck, J. G. Horstmann, T. Diekmann, M. Sivis, S. Schramm, K. Rossnagel, S. Schäfer, and C. Ropers, Phase ordering of charge density waves traced by ultrafast low-energy electron diffraction, *Nat. Phys.* **14**, 184 (2018).
- [18] S. Hellmann, T. Rohwer, M. Kalläne, K. Hanff, C. Sohrt, A. Stange, A. Carr, M. M. Murnane, H. C. Kapteyn, L. Kipp, M. Bauer, and K. Rossnagel, Time-domain classification of charge-density-wave insulators, *Nat. Commun.* **3**, 1069 (2012).
- [19] M. J. Hollander, Y. Liu, W.-J. Lu, L.-J. Li, Y.-P. Sun, J. A. Robinson, and S. Datta, Electrically Driven Reversible Insulator-Metal Phase Transition in 1T-TaS<sub>2</sub>, *Nano Lett.* **15**, 1861 (2015).
- [20] I. Vaskivskiy, I. A. Mihailovic, S. Brazovskii, J. Gospodaric, T. Mertelj, D. Svetin, P. Sutar, D. Mihailovic, Fast electronic resistance switching involving hidden charge density wave states, *Nat. Commun.* **7**, 11442 (2016).
- [21] B. Grisafe, R. Zhao, R. K. Ghosh, J. A. Robinson, and S. Datta, Electrically triggered insulator-to-metal phase transition in two-dimensional (2D) heterostructures, *Appl. Phys. Lett.* **113**, 142101 (2018).
- [22] Y. Li, K.-A. N. Duerloo, K. Wauson, and E. J. Reed, Structural semiconductor-to-semimetal phase transition in two-dimensional materials induced by electrostatic gating, *Nat. Commun.* **7**, 10671 (2016).
- [23] A. K. Geremew, S. Rumyantsev, F. Kargar, B. Debnath, A. Nosek, M. A. Bloodgood, M. Bockrath, T.T. Salguero, R. K. Lake, and A. A. Balandin, Bias-Voltage Driven Switching of the Charge-Density-Wave and Normal Metallic Phases in 1T-TaS<sub>2</sub> Thin-Film Devices, *ACS Nano* **13**, 7231 (2019).
- [24] S. Zheng, F. Liu, C. Zhu, Z. Liu, and H. J. Fan, Room-temperature electrically driven phase transition of two-dimensional 1T-TaS<sub>2</sub> layers, *Nanoscale* **9**, 2436 (2017).
- [25] G. Liu, B. Debnath, T. R. Pope, T. T. Salguero, R. K. Lake, and A. A. Balandin, A charge-density-wave oscillator based on an integrated tantalum disulfide-boron nitride-graphene device operating at room temperature, *Nat. Nanotechnol.* **11**, 845 (2016).
- [26] A. G. Khitun, A. K. Geremew, and A. A. Balandin, Transistor-Less Logic Circuits Implemented With 2-D Charge Density Wave Devices, *IEEE Electron Device Lett.* **39**, 1449 (2018).
- [27] R. Waser and M. Aono, Nanoionics-based resistive switching memories, *Nat. Mater.* **6**, 833 (2007).
- [28] A. Sawa, Resistive switching in transition metal oxides, *Mater. Today* **11**, 28 (2008).
- [29] R. Waser, R. Dittmann, G. Staikov, K. Szot, Redox-based resistive switching memories - Nanoionic mechanisms, prospects, and challenges, *Adv. Mater.* **21**, 2632 (2009).
- [30] K. M. Kim, D. S. Jeong, and C. S. Hwang, Nanofilamentary resistive switching in binary oxide system; a review on the present status and outlook, *Nanotechnology* **22**, 254002 (2011).
- [31] D. S. Jeong, R. Thomas, R. S. Katiyar, J. F. Scott, H. Kohlstedt, A. Petraru, and C. S. Hwang, Emerging memories: resistive switching mechanisms and current status, *Rep. Prog. Phys.* **75**, 076502 (2012).
- [32] J. S. Lee, S. Lee, and T. W. Noh, Resistive switching phenomena: A review of statistical physics approaches, *Appl. Phys. Rev.* **2**, 031303 (2015).
- [33] E. Janod, J. Tranchant, B. Corraze, M. Querre, P. Stollari, M. Rozenberg, T. Cren, D. Roditchev, V. T. Phuoc, M.-P. Besland, and L. Cario, Resistive switching in Mott insulators and correlated systems, *Adv. Funct. Mater.* **25**, 6287 (2015).
- [34] T. Holstein, Studies of polaron motion: Part I. The molecular-crystal model, *Ann. Phys.* **8**, 325 (1959).
- [35] J. Bonca, S. A. Trugman, and I. Batistić, Holstein polaron, *Phys. Rev. B* **60**, 1633 (1999).
- [36] D. Golez, J. Bonca, L. Vidmar, and S. A. Trugman, Relaxation Dynamics of the Holstein Polaron, *Phys. Rev. Lett.* **109**, 236402 (2012).
- [37] A. S. Mishchenko, N. Nagaosa, G. De Filippis, A. de Candia, and V. Cataudella, Mobility of Holstein Polaron at Finite Temperature: An Unbiased Approach, *Phys. Rev. Lett.* **114**, 146401 (2015).
- [38] Y.-X. Zhang, W.-T. Chiu, N. C. Costa, G. G. Batrouni, and R. T. Scalettar, Charge Order in the Holstein Model on a Honeycomb Lattice, *Phys. Rev. Lett.* **122**, 077602 (2019).
- [39] N. C. Costa, T. Blommel, W.-T. Chiu, G. Batrouni, and R. T. Scalettar, Phonon Dispersion and the Competition between Pairing and Charge Order, *Phys. Rev. Lett.* **120**, 187003 (2018).
- [40] F. Marsiglio, Pairing and charge-density-wave correla-

- tions in the Holstein model at half-filling, *Phys. Rev. B* **42**, 2416 (1990).
- [41] M. Vekic, R. M. Noack, and S. R. White, Charge-density waves versus superconductivity in the Holstein model with next-nearest-neighbor hopping, *Phys. Rev. B* **46**, 271 (1992).
- [42] H. Zheng and S. Y. Zhu, Charge-density-wave and superconducting states in the Holstein model on a square lattice, *Phys. Rev. B* **55**, 3803 (1997).
- [43] B. Cohen-Stead, K. Barros, Z. Meng, C. Chen, R. T. Scalettar, and G. G. Batrouni, Langevin simulations of the half-filled cubic Holstein model, *Phys. Rev. B* **102**, 161108 (2020).
- [44] A. Goetz, S. Beyl, M. Hohenadler, and F. F. Assaad, Langevin dynamics simulations of the two-dimensional Su-Schrieffer-Heeger model, arXiv:2102.08899 (2021).
- [45] K. Michielsen, H. De Raedt, Quantum molecular dynamics study of the Su-Schrieffer-Heeger model, *Z. Phys. B* **103**, 391 (1997).
- [46] D. Marx and J. Hutter, *Ab initio molecular dynamics: basic theory and advanced methods* (Cambridge University Press, Cambridge, 2009).
- [47] M. Di Ventura and S. T. Pantelides, Hellmann-Feynman theorem and the definition of forces in quantum time-dependent and transport problems, *Phys. Rev. B* **61**, 16207 (2000).
- [48] T. N. Todorov, Time-dependent tight-binding, *J. Phys.: Condens. Matter* **13**, 10125 (2001).
- [49] J.-T.Lü, M. Brandbyge, P. Hedegard, T. N. Todorov, and D. Dundas, Current-induced atomic dynamics, instabilities, and Raman signals: Quasiclassical Langevin equation approach, *Phys. Rev. B* **85**, 245444 (2012).
- [50] T. N. Todorov, D. Dundas, and E. J. McEniry, Nonconservative generalized current-induced forces, *Phys. Rev. B* **81**, 075416 (2010).
- [51] D. Dundas, E. J. McEniry, and T. N. Todorov, Current-driven atomic waterwheels, *Nat. Nanotech.* **4**, 99 (2009).
- [52] Y. Meir and N. S. Wingreen, Landauer formula for the current through an interacting electron region, *Phys. Rev. Lett.* **68**, 2512 (1992).
- [53] A.-P. Jauho, N. S. Wingreen, Y. Meir, Time-dependent transport in interacting and noninteracting resonant-tunneling systems, *Phys. Rev. B* **50**, 5528 (1994).
- [54] H. Haug and A.-P. Jauho, *Quantum Kinetics in Transport and Optics of Semiconductors*, Springer Series in Solid-State Sciences **123** (Springer-Verlag, Berlin, 2008).
- [55] M. Di Ventura, *Electrical Transport in Nanoscale Systems* (Cambridge University Press, Cambridge, 2008).
- [56] J. Zhong and H.-B. Schüttler, Polaronic anharmonicity in the Holstein-Hubbard model, *Phys. Rev. Lett.* **69**, 1600 (1992).
- [57] M. Weber and M. Hohenadler, Two-dimensional Holstein-Hubbard model: Critical temperature, Ising universality, and bipolaron liquid, *Phys. Rev. B* **98**, 085405 (2018).
- [58] P. Ribeiro, A. E. Antipov, and A. N. Rubtsov, Nonequilibrium breakdown of a correlated insulator through pattern formation, *Phys. Rev. B* **93**, 144305 (2016).
- [59] J. Li, C. Aron, G. Kotliar, and J. E. Han, Microscopic theory of resistive switching in ordered insulators: Electronic versus thermal mechanisms, *Nano Lett.* **17**, 2994 (2017).
- [60] A. Dutta and P. Majumdar, Spatial behavior in a Mott insulator near the voltage-driven resistive transition, *Phys. Rev. B* **101**, 245155 (2020).